


Article

The Design and Experimentation of a Wing-Shaped Stubble-Breaking Device for Maize Stubbles

Xuanting Liu ^{1,2}, Hongyan Qi ³, Shuo Wang ^{1,2}, Zihe Xu ^{1,2}, Peng Gao ^{1,2} , Daping Fu ⁴ and Yunhai Ma ^{1,2,*}

¹ Key Laboratory of Bionic Engineering, Ministry of Education, Jilin University, Changchun 130022, China; xuanting120@mails.jlu.edu.cn (X.L.); wangshuo21@mails.jlu.edu.cn (S.W.); zhxu21@mails.jlu.edu.cn (Z.X.); penggao15@mails.jlu.edu.cn (P.G.)

² College of Biological and Agricultural Engineering, Jilin University, Changchun 130022, China

³ College of Mechanical Engineering, Hunan University of Arts and Science, Changde 415000, China; qhy18@mails.jlu.edu.cn

⁴ College of Engineering Technology, Jilin Agricultural University, Changchun 250100, China; fudaping@jlu.edu.cn

* Correspondence: myh@jlu.edu.cn

Abstract: To achieve high-quality no-till seeding, a wing-shaped stubble-breaking device with excellent stubble-breaking performance was designed for maize stubble. A model of maize stubble was developed based on the Discrete Element Method (DEM) and verified through soil bin tests. The DEM model was used to optimize the design parameters of the device and to investigate the interaction between the blades and the maize stubble during the stubble-breaking process. Field experiments were conducted to evaluate the performance of the device. The results indicated that the DEM model was accurate; when the optimal design parameters of the wing-shaped stubble-breaking device were a 37° slide cutting angle, 31° pitching angle, and 50 mm wing width, the average torque was 41.26 N·m, the soil breakage rate was 85.68%, and the soil backfill rate was 71.65%; the wing-shaped stubble-breaking device could separate the inside and outside of the strip tillage area and cut maize stubbles and soil blocks twice, thus having excellent stubble-breaking performance. This study provided an effective and feasible method for designing stubble-breaking devices and studying the interaction between blades, soil, and roots, which improved soil tillage theory and was beneficial in promoting conservation tillage technology.



Citation: Liu, X.; Qi, H.; Wang, S.; Xu, Z.; Gao, P.; Fu, D.; Ma, Y. The Design and Experimentation of a Wing-Shaped Stubble-Breaking Device for Maize Stubbles. *Agriculture* **2024**, *14*, 2108. <https://doi.org/10.3390/agriculture14122108>

Academic Editor: Valentin Vlăduț

Received: 22 October 2024

Revised: 19 November 2024

Accepted: 20 November 2024

Published: 22 November 2024



Copyright: © 2024 by the authors. Licensee MDPI, Basel, Switzerland. This article is an open access article distributed under the terms and conditions of the Creative Commons Attribution (CC BY) license (<https://creativecommons.org/licenses/by/4.0/>).

Keywords: wing-shaped stubble-breaking device; discrete element method; maize stubble; average torque; soil breakage rate; soil backfill rate

1. Introduction

To solve problems such as soil erosion and degradation in traditional tillage, conservation tillage techniques have been widely promoted in northeast China. After years of development, conservation tillage has become a sustainable tillage method suitable for local agricultural tillage, which reduces soil erosion, protects soil organic matter, and increases crop yields [1,2]. However, due to the cold and dry climate in northeast China, crop residues are difficult to rot and break, especially stubbles with stable and sturdy structures. During no-till seeding, no-till planters usually encounter problems such as severe blockages and a poor seedbed environment. These problems significantly affect the quality of the no-till seeding operation and have become one of the major bottlenecks limiting the development of conservation tillage [3,4].

To efficiently remove stubbles and create a favorable seeding environment, no-till planters are usually equipped with stubble-breaking devices [3,4]. The driving-type stubble-breaking device is commonly used in Northeast China. Although this kind of stubble-breaking device can effectively prevent blockages, it has problems such as a high soil disturbance and energy consumption [3,4]. At present, the commonly used stubble-breaking

devices are still designed based on the theory of interaction between tillage components and soil [5,6]. Therefore, the current design standards are not fully applicable to the design of no-till stubble-breaking devices, and it is necessary to design a stubble-breaking device for stubble.

To design a stubble-breaking device suitable for no-till seeding and improve its performance, many researchers have conducted research on stubble-breaking devices. Jia et al. [7] designed a bionic dynamic stubble-breaking device with forward and reverse rotation functions, which improved the stubble-breaking rate by 8.6% to 13.5% and reduced the torque by 19.5% to 21.8% compared to the driven-type notched disk; Jiang et al. [8] designed a corn stalk and residue-cutting device which could dig out maize stubbles and reduce the soil disturbance; Yang et al. [9,10] investigated the performance of blades with different geometries and designed a strip anti-blocking device by combining hoe blades and rotary blades reasonably, which could create a better seeding environment and have a lower soil disturbance. These studies used experimental methods to obtain data and build empirical models. The model was used to optimize the design parameters of the stubble-breaking device and improve its performance. However, the experimental method is expensive and the experimental conditions are difficult to control, which makes it difficult to obtain data with low errors.

With the continuous development of computer technology and numerical simulation theory, numerical simulation has become an effective method for investigating the interaction between tillage components, soil, and crop residues. Compared with experimental methods, numerical simulation methods have the advantages of accurate, efficient, reliable, and reproducible test results [11]. The DEM is a discontinuous numerical method for simulating the mechanical behavior of materials, which has a high degree of accuracy in simulating the deformation, failure, and motion behavior of materials. It has been widely used to solve various mechanical problems in agricultural production. Many researchers have used the DEM to study the mechanical properties of plant stems [12], soil [13], and crop seeds [14]. They have also studied tillage operations such as rotary tillage [15] and deep loosening [16,17]. To design high-performance tillage equipment, many researchers have used the DEM to study the interaction between tillage components and crop residues. Zeng et al. [18,19] used a three-dimensional particle flow code to simulate the effects of chisel operations on soil and residue displacement at different speeds. Zhang et al. [20–22] developed a DEM model of maize stubbles and optimized the operating parameters of the device implementing a disk and the anti-blocking device; Tamas et al. [23] developed a DEM model of the root–soil complex and studied the effect of the roots on the resistance of sweeping blades; Qian et al. [24] developed a DEM model of sugarcane stubble and studied the interaction between the blade and the sugarcane stubble. The above research indicated that the DEM was suitable for simulating the interactions between tillage components, soil, and maize stubbles.

In this study, a wing-shaped stubble-breaking device was designed for the maize stubble. A DEM model of the maize stubble was developed to optimize the design parameters of the wing-shaped stubble-breaking device (the sliding cutting angle, pitch angle, and wing width). The accuracy of the DEM model was verified through soil bin tests and the performance of the stubble-breaking device was evaluated through field experiments. This study provided a new method to design a stubble-breaking device and promote conservation tillage techniques.

2. Design of Wing-Shaped Stubble-Breaking Device

Inspired by Lee and Matin's research on strip tillage blades [25–29], a wing-shaped stubble-breaking device (Figure 1a) was designed to decrease the stubble-breaking torque, avoid a higher soil disturbance, and improve the breakage rate of soil blocks and stubbles. The wing-shaped stubble-breaking device consisted of a frame and a transmission system. The wing-shaped blade set (Figure 2) consisted of three adjustable holding flanges (Figure 2a), wing-shaped blades (Figure 2b), and straight blades (Figure 2c). The spacing

between the three coaxial adjustable holding flanges was 40 mm. The straight blades were installed on both sides of the wing-shaped blade set, and the wing-shaped blades were installed on the middle adjustable holding flange. The blades in the same blade set were evenly arranged, and the blades in adjacent blade sets were evenly staggered. Wing-shaped blades had tangent blade edges and side blade edges. The two types of blade edges were perpendicular to each other in the plane. The straight blade could shape the walls of the strip tillage area, separate tilled and untilled areas, and reduce the impact of root anchoring on the torque [30]. The wing-shaped blades could break maize stubbles and soil blocks inside the strip tillage area, which could help to increase the soil breakage rate (Figure 1b). Summarizing previous research, McKyes et al. [31] found that as the contact area between the tillage components and the soil increased, the pure cutting force and tillage resistance increased. When multiple blades of the stubble-breaking device entered the soil simultaneously, the contact area between the blades and the soil increased, resulting in higher resistance and energy consumption. Moreover, since the torque of the stubble-breaking device was the sum of the torque contributed by each blade, if there were too many blades arranged on the flange, the torque would increase significantly. Therefore, only two blades were installed on each flange of the wing-shaped blade set.

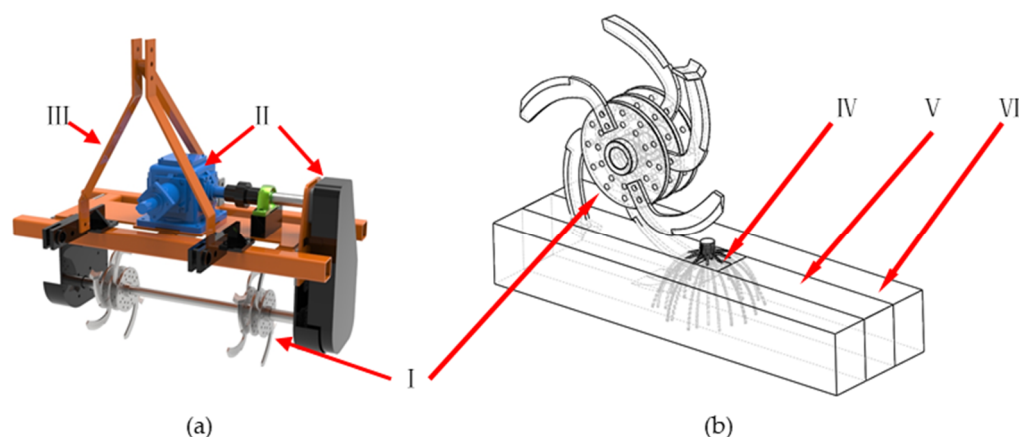


Figure 1. Design of wing-shaped stubble-breaking device: (a) Wing-shaped stubble-breaking device: I: wing-shaped blade set; II: transmission system; III: frame. (b) Operating principle of wing-shaped stubble-breaking device: IV: maize stubble; V: strip tillage area; VI: untilled area.

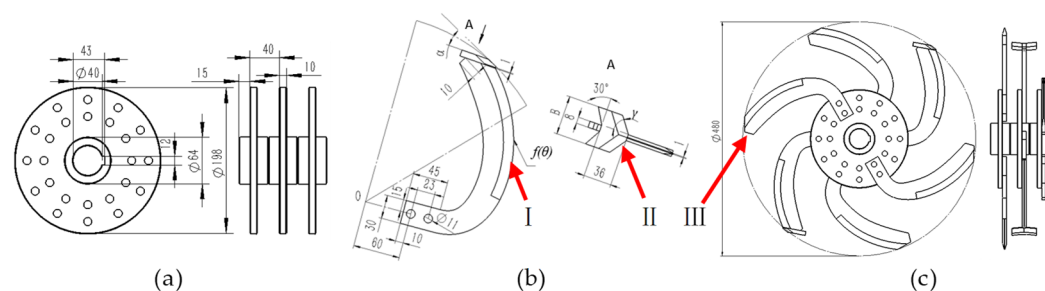


Figure 2. Design of wing-shaped blade set: (a) adjustable holding flange; (b) wing-shaped blade: I: side blade; II: tangent blade; (c) wing-shaped blade set: III: straight blade.

The key design parameters of the wing-shaped blade included the slide cutting angle ζ of the tangent blade and the side blade, the pitching angle α of the wing, and the wing width B . The width of the wing (Figure 2b) was defined as the wing width B . According to the research of Matin et al. [29], the width of the lateral portion of a conventional blade (bent blade) could significantly affect the soil disturbance and torque. As the wing width increased, the lateral width of the blade also increased. The thickness of the blade was 8 mm, and the width of the strip tillage area was 80 mm. A wide wing could cause a

blockage, while a narrow wing had a weaker stubble-breaking ability. Therefore, the wing width was determined to be selected within the range of 30 mm to 70 mm. The pitching angle α was defined as the angle between the tangent of the blade rotation circle and the plane where the wing-shaped blade was located (Figure 2b). The clearance angle δ was defined as the angle between the surface of the wing-shaped blade and the tangent line of the blade endpoint motion trajectory (Figure 3). According to the research of Matin and Zhao et al. [27,32], as the clearance angle decreases, the risk of interference between the straight blade and the untilled area increases, which increases the torque and brings risks of device vibration. Usually, the clearance angle should be within the range of 20° to 30°. According to the research of Gill, W.R. et al. [33], the wing-shaped blade with high pitching angles had a greater soil-facing surface, which could improve its ability to break soil blocks and stubbles, while also increasing the soil disturbance sand torque. The wing-shaped blade with a lower pitching angle had a lower soil-facing surface, which could reduce the soil disturbance and torque, but its stubble-breaking ability was weaker. Because both the higher and lower pitching angles were not conducive to stubble-breaking operations, the pitching angle was determined to be 10° to 50°.

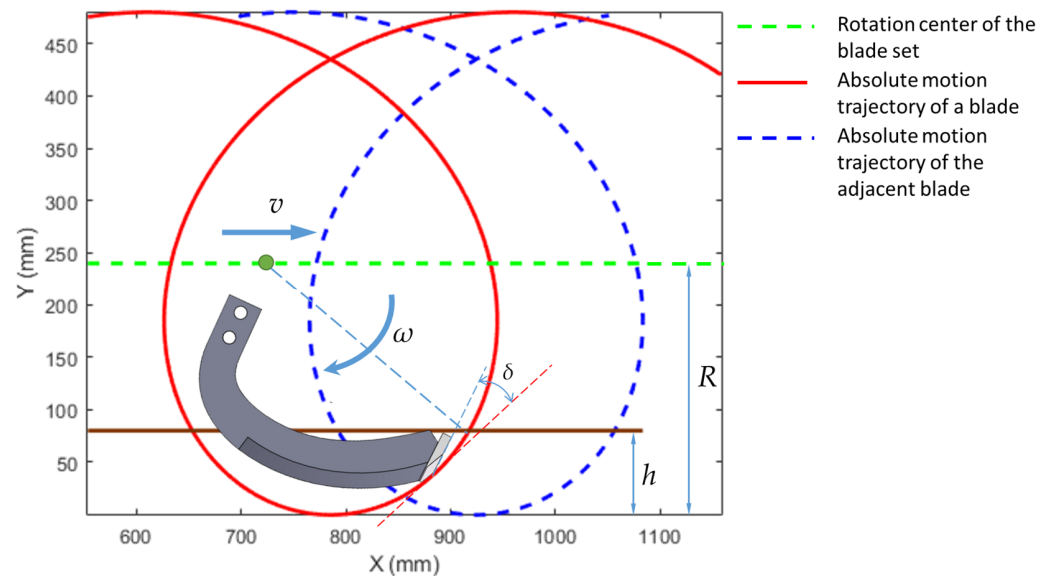


Figure 3. Motion trajectory of wing-shaped blade.

The slide cutting angle was defined as the angle between the speed direction and the normal direction of the blade edge. According to the research of Zhao et al. [15], the slide cutting angle of blade edge curves could significantly influence the torque and an Archimedean equal entry spiral could be used to design the side blade, which could reduce the torque. The curve of the side blade ρ can be expressed by the following equations:

$$\rho = \rho_0 + k\theta \tag{1}$$

$$\rho_0 = \sqrt{R^2 + S^2 - 2S\sqrt{2Rh - h^2}} \tag{2}$$

$$\theta_n = \frac{\rho_n - \rho_0}{\rho_0} \tan \tau_n \tag{3}$$

where θ is the polar angle at any point on the spiral, rad; k is the increment of the polar diameter, mm/rad; ρ_0 is the polar diameter at the starting point of the spiral, mm; S is the design cutting intercept; R is the rotation radius; h is the design plowing depth, mm; θ_n is the polar angle at the endpoint of the spiral, rad; and τ_n is the slide cutting angle at the endpoint of the spiral, rad.

The dynamic slide cutting angle β of the tangent blade is

$$\beta = \arctg \frac{v_t}{v_n} \quad (4)$$

$$v_t = v \cos \varphi \sin \gamma \quad (5)$$

$$v_n = v \cos \varphi \cos \gamma \quad (6)$$

where v is the actual velocity at the cutting edge of the tangent blade, m/s; v_t is the partial velocity of the actual velocity in the tangential direction of the tangent blade, m/s; v_n is the partial velocity of the actual velocity in the normal direction of the tangent blade, m/s; φ is the angle between plane I (Figure 4) where the tangent blade is located and plane II (Figure 4) where the instantaneous velocity of the tangent blade edge is located, °; and 2γ is the tangent blade angle, °.

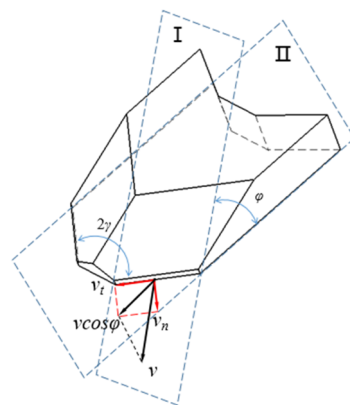


Figure 4. The design of the dynamic slide cutting angle: I: the plane where the instantaneous velocity of the tangent blade edge is located; II: the plane where the tangent blade is located.

To reduce the torque of the wing-shaped stubble-breaking device, it was necessary to optimize the dynamic sliding cutting angle of the tangent blade and the slide cutting angle of the spiral endpoint of the side blade. These two angles are called slide cutting angles. According to the research of Zhao et al. [34], the static friction angle between the blade and the maize root was 30° to 50°. However, as the slide cutting angle increased, the blade edge became longer, and multiple blades would enter the soil at the same time, which increased the torque. Therefore, the slide cutting angle of the wing-shaped blade should be within the range of 0° to 50°.

3. Discrete Element Simulation

3.1. Establishment of Discrete Element Model

To evaluate the performance of the stubble-breaking device, a DEM model (Figure 5) was developed using EDEM 2018 (Altair Engineering Inc., Troy, MI, USA), which consisted of the stubble-breaking blade, maize roots, soil, and soil bin. Soil particles with a radius of 2 mm were randomly generated and freely dropped into a soil bin model with a length of 1000 mm, a width of 400 mm, and a depth of 200 mm. The maize root model was created using SolidWorks 2018 (Dassault Systems, Suresnes, France) and imported into EDEM 2018. It was filled with root particles with a radius of 1.5 mm using the EDEM API [20]. According to the research of Zhang and Zhao et al. [20,34], basic physical parameters, Hertz–Mindlin bonding parameters (Table 1), and contact parameters (Table 2) were assigned to the particles of the roots, soil, and blade. The working depth of the stubble-breaking device was 80 mm, the rotation speed was 300 rpm, and the forward speed was 0.8 m/s. The calculation grid size was 4.5 mm, the Rayleigh time step size was 1.2×10^{-6} s, and the target save interval was 0.001 s.

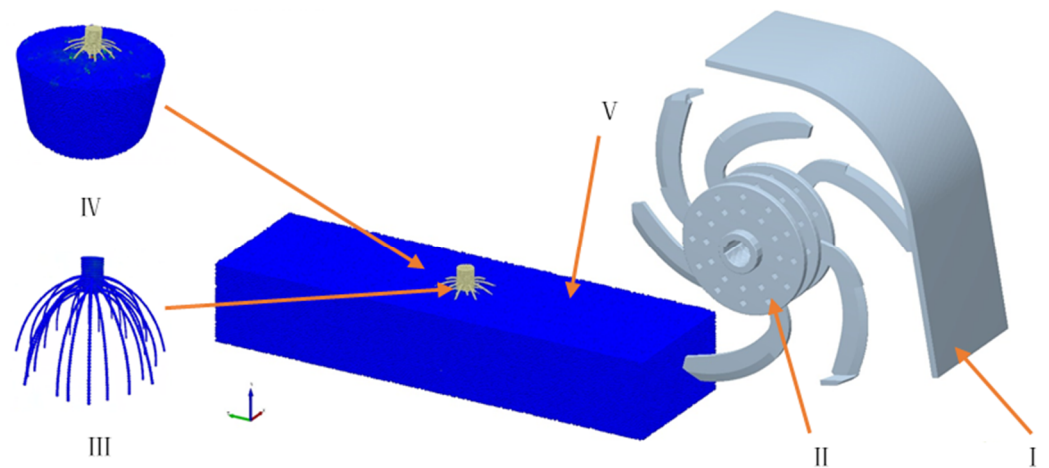


Figure 5. DEM model of strip stubble-breaking operation: I: retaining plate; II: strip stubble-breaking blade set; III: maize stubble; IV: maize roots; V: soil.

Table 1. Key parameters of the DEM model.

Parameter	Material	Value
Density (kg/m^3)	soil	107
	root	2620
Poisson's ratio	65Mn steel	7650
	soil	0.40
	root	0.35
Young's modulus (Pa)	65Mn steel	0.35
	soil	5.10×10^7
	root	7.02×10^7
Normal stiffness of bond (N/m^3)	65Mn steel	2.50×10^{11}
	soil–soil	1.19×10^7
	root–root	7.74×10^9
Critical stresses of bond (Pa)	soil–root	4.00×10^7
	soil–soil	1.00×10^7
	root–root	7.00×10^7
Bond disk radius (mm)	soil–root	1.00×10^7
	soil–soil	0.66
	root–root	1.56
Surface energy coefficients (J/m^2)	soil–root	1.10
	soil–soil	3.38
	root–root	3.38

Table 2. Key friction parameters of the DEM model.

Parameter	Material	Value
Coefficient of restitution	soil–soil	0.60
	root–root	0.65
	soil–root	0.65
	soil–steel	0.60
	root–steel	0.32
Coefficient of static friction	soil–soil	0.60
	root–root	0.62
	soil–root	0.55
	soil–steel	0.40
	root–steel	0.60

Table 2. Cont.

Parameter	Material	Value
Coefficient of rolling friction	soil–soil	0.30
	root–root	0.25
	soil–root	0.32
	soil–steel	0.25
	root–steel	0.20

3.2. Verification Experiment

3.2.1. Material and Equipment

The maize stubble (Figure 6a) used in the soil bin test was collected in Siping, Jilin Province ($43^{\circ}12'10''$ N, $124^{\circ}22'18''$ E) on 1 October 2023. The maize variety was Zhengdan 958, and the maize roots were mainly distributed in the soil layer at a depth of 0 to 100 mm. The stem diameter of the collected maize stubble was 25 ± 5 mm, and the size of the underground area was $300 \text{ mm} \times 300 \text{ mm} \times 200 \text{ mm}$. The density of the roots was 107 kg/m^3 , and the wet moisture content was 64.78% to 85.60%. The soil was black loam. The average soil compaction of the soil layer was 1.12 MPa at a depth of 0 to 100 mm, the average bulk density of the soil layer was 2600 kg/m^3 , and the average soil moisture content was 19.30%.

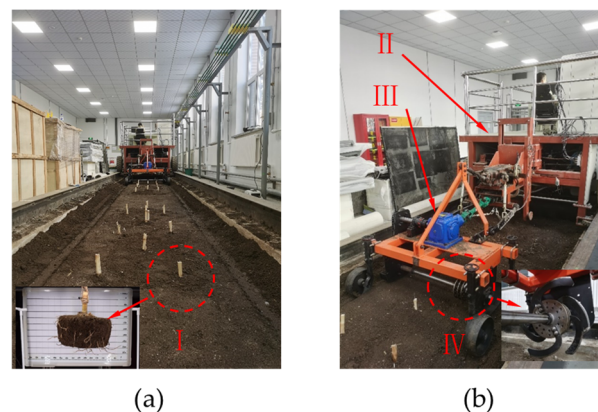


Figure 6. Experimental equipment of soil bin test: (a) soil bin: I: maize stubble; (b) experimental equipment: II: soil bin test system; III: wing-shaped stubble-breaking device; IV: stubble-breaking blade set.

The soil bin test was conducted in the soil bin laboratory (soil bin length of 30 m, width of 4 m) of Jilin University. The soil preparation process included breaking and leveling the soil, watering to adjust the soil moisture content, initially compacting the soil, burying the stubbles, and compacting the soil. The soil moisture content was adjusted to $19 \pm 0.5\%$ and the soil compaction was adjusted to 1.2 ± 0.2 MPa. To ensure that there was no interference between each set of experiments and to efficiently complete the experiments, the soil bin test was divided into three parts. The acceleration section and deceleration section were located at both ends of the stable section, each with a length of 5 m. The length of the stable section was 6 m, which was for recording experimental data. Three rows of stubbles were placed in the stable section along the length of the soil bin, with 0.5 m between each row and 0.5 m between each column (Figure 6a). The main experimental equipment was the soil bin test system and the stubble-breaking device (Figure 6b). The soil bin test system could measure the torque of the equipment in real time. The bent blade (Figure 7a), straight blade (Figure 7b), and wing-shaped blade (Figure 7c) used in the experiment were all made of 65Mn. The slide cutting angle of the straight blade was 30° , the pitching angle of the wing blade was 30° , and the wing width was 50 mm.

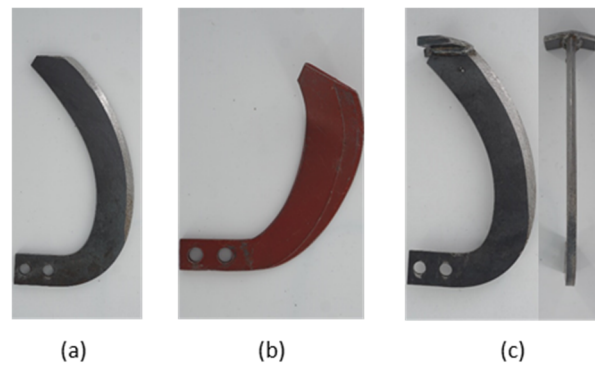


Figure 7. Stubble-breaking blade: (a) straight blade; (b) bent blade; (c) wing-shaped blade.

3.2.2. Experimental Method

To verify the DEM model and investigate the performance of wing-shaped blade sets and other general blade sets, three types of stubble-breaking blade sets were designed (Figure 8). The blades of the straight blade set (Figure 8a) and the bent blade (Figure 8b) set were only installed on the two-sided adjustable holding flange, with a configuration of 2. The average torque, soil breakage rate, and soil backfill rate were used to verify the DEM model and evaluate the three types of stubble-breaking blade sets. The measurement and evaluation methods are as follows.

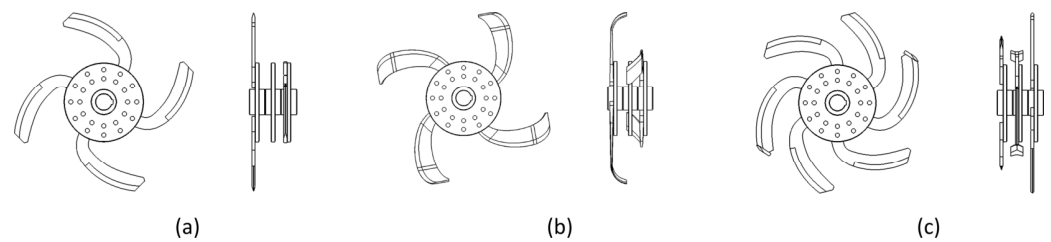


Figure 8. Strip blade set: (a) straight blade set, (b) bent blade set, (c) wing-shaped blade set.

Average torque: the torque of the stubble-breaking device can be output by EDEM 2018 and soil bin test system. The average torque was defined as the average torque from the beginning to the end of the stubble-breaking process. The average torque was calculated using Equation (7).

$$T = \frac{1}{t_2 - t_1} \int_{t_1}^{t_2} T(t) dt \quad (7)$$

where $T(t)$ is the instantaneous torque at each time point, N·m, and t_1 and t_2 are the starting and ending time points of the stubble-breaking process, s.

Soil breakage rate: when the force applied by the blade to the soil is greater than the bonding force between soil particles, the bonds between soil particles break. Therefore, by using the Grid Bin Group function of EDEM 2018, the number of broken and intact bonds in a specific area could be output and helped evaluate soil breakage. The soil breakage rate was calculated using Equation (8).

$$I = \frac{N_b}{N_b + N_i} \times 100\% \quad (8)$$

where I is the soil breakage rate, %; N_b is the number of broken bonds of the soil particles in the tilled area; and N_i is the number of intact bonds of the soil particles in the tilled area.

Soil backfill rate: the soil backfill rate was defined as the ratio of the number of soil particles in the seedbed before and after tillage. By using the Grid Bin Group function of

EDEM, the number of soil particles in the area before and after tillage could be output. The soil backfill rate was calculated using Equation (9).

$$P = \frac{N_a}{N_b} \times 100\% \quad (9)$$

where P is the soil backfill rate, %; N_a is the number of soil particles in the seedbed after tillage; and N_b is the number of soil particles in the selected area before tillage.

To verify the DEM model, it was necessary to measure the soil backfill rate in the soil bin test. Here, the soil backfill rate was defined as the ratio of the weight of undisturbed soil to the weight of disturbed soil in the seedbed. The higher the soil backfill rate, the more soil comes into contact with seeds, which is more conducive to seed germination. When measuring the soil backfill rate, a plastic film (<0.2 mm thick) was used to gently spread on the cleaned test area, and standard sand with a dry density of 1280 kg/m³ and a particle diameter of <1 mm was used to gently sprinkle along the boundary of the seedbed onto the plastic film until it was level with the surface of the test area. The standard sand was taken out to calculate the volume of the seedbed in the testing area. The soil backfill rate was calculated using Equations (10) and (11):

$$F = \frac{W}{V\rho_w} \quad (10)$$

$$V = \frac{M}{\rho_s} \quad (11)$$

where F is the soil backfill rate, %; W is the dry weight of the soil remaining in the seedbed after tillage, kg; ρ_w is the soil bulk density, kg·m⁻³; V is the volume of the seedbed in the test area, m³; M is the standard sand mass in the seeding bed, kg; and ρ_s is the standard sand density, kg·m⁻³.

According to the research of Liu et al. [30], the resistance of blades is directly related to the deformation of roots and soil. To explore the interaction mechanism between the blade set and maize stubbles, it was necessary to use the DEM to analyze the deformation of the roots and soil.

3.3. Response Surface Experiment

To improve the performance of the wing-shaped blade set, it was necessary to optimize its design parameters. The Box–Behnken method optimized the parameters and determined the optimal parameter combination. There were 15 response surface experiments, including 3 central experiments, mainly used to estimate experimental errors. Each parameter was set at three levels: low (−1), middle (0), and high (1). The factors and levels are listed in Table 3. The response values were the average torque (Y_1), soil breakage rate (Y_2), and soil backfill rate (Y_3).

Table 3. Coding of regression experiment factors.

Levels	Factors		
	Slide Cutting Angle X_1 /(°)	Pitching Angle X_2 /(°)	Wing Width X_3 /(mm)
−1	0	10	30
0	25	30	50
1	50	50	70

4. Field Experiments

The field experiment was conducted to evaluate the performance of the wing-shaped stubble-breaking device.

4.1. Materials and Equipment

The field experiment was conducted on 28 October 2023, at the stubble collection site. This field implemented conservation tillage techniques year-round (Figure 9a). The average soil compaction of the soil was 1.2 MPa at a depth of 0 to 100 mm, the average bulk density of the soil was 2430 kg/m³, and the average moisture content of the soil was 20.45%. The density of the roots was 173 kg/m³, and the wet moisture content of the roots was 60.68% to 95.45%.



Figure 9. (a) Field experiment site and (b) experimental equipment: I: torque sensor.

The model of the experimental tractor was a Kubota M704, and the stubble-breaking device was the same as the soil bin used (Figure 9b). The torque sensor (Figure 9b) was used to measure the torque. The tractor's power output shaft was connected to a stubble-breaking device through the torque sensor. The real-time torque could be output and transmitted to the computer.

4.2. Experiment Method

The field experiment required that the working depth of the stubble-breaking device be 80 mm, the rotation speed be 300 rpm, and the forward speed be 0.8 m/s. The length of the experimental area was 100 m, with rows of stubbles. Each experimental area was divided into acceleration and braking areas with lengths of 10 m at both ends and a stable operation area with a length of 80 m in the middle. The data of stable operation areas were collected to analyze. The performances of the wing-shaped blade set, bent blade set, and straight blade set were evaluated using the average torque, soil backfill rate, and soil breakage rate. The measurement methods of the average torque and soil backfill rate are described in Section 3.2.1. The measurement method of the soil breakage rate is as follows:

Soil breakage rate: the size of soil blocks within the strip area of 500 mm × 80 mm were measured. The ratio of the soil blocks with the longest side being less than 40 mm in this area to the total soil mass was the soil breakage rate. The soil breakage rate was calculated using Equation (12).

$$W = \left(1 - \frac{M_q}{M_h}\right) \times 100\% \quad (12)$$

where W is the soil breakage rate; M_q is the mass of soil blocks with the longest side being greater than 40 mm, g; and M_h is the measurement of the soil mass of all areas in the measurement area, g.

The performance parameters of each blade set were measured five times, and the average value of each parameter was taken as the final result.

5. Results and Discussion

5.1. DEM Simulation Analysis

5.1.1. Model Verification and Analysis

To verify the model, the results of the soil bin test were compared with those of the simulation (Table 4). The maximum relative deviation of the average torque and soil backfill rate was less than 15%. The deviation could be attributed to the complex field environment and variations in maize growth. These results indicated that the model was reliable.

Table 4. Verification test results.

Indicators	Average Torque (N·m)			Soil Backfill Rate (%)			Soil Breakage Rate (%)
	Simulation	Test	Deviation	Simulation	Test	Deviation	Simulation
Straight	23.86	27.52	14.25%	80.45	74.47	7.72%	30.26
Bent	35.23	38.56	9.03%	54.53	47.62	13.53%	72.56
Wing	39.72	42.26	6.20%	71.57	70.65	1.29%	78.68

The simulation results (Table 4) showed that compared with the straight blade set and the bent blade set, the average torque of the wing-shaped blade set increased by 36.88% and 4.56%, the soil breakage rate increased by 61.54% and 7.78%, and the soil backfill rate decreased by 3.6% and increased by 29.77%. Obviously, the wing-shaped blade set had a higher soil breakage rate and soil backfill rate. However, due to the addition of two more blades compared to the general blade set, the average torque of the wing-shaped blade set was higher. In summary, the wing-shaped blade set has better performance than the general blade set. To reduce the average torque of wing-shaped blade sets and improve the soil breakage rate and backfill rate, the wing-shaped blade set needs further design optimization.

The discrete element velocity cloud image showed that the bent blade set threw a large amount of soil outside the strip tillage area (Figure 10a), while the wing-shaped blade set (Figure 10b) and straight blade set (Figure 10c) threw out less soil. The soil disturbance of each blade set was related to the structure and assembly method of the blades. The bent blade had both tangent and side blade edges and had a bending structure. The tangent and side blade edges could successively cut the soil block and stubble in the strip tillage area within one rotation cycle. At the same time, it also disturbed the soil outside the strip tillage area (Figure 11a). Therefore, the bent blade set had better stubble-breaking performance but was not conducive to reducing the soil disturbance; the straight blade did not have a bending structure and only cut soil blocks and stubbles within a rotating plane. Therefore, a straight blade could easily break stubbles and separate the inside and outside of the strip tillage area from each other (Figure 11b). Therefore, the straight blade set had less soil disturbance and was more suitable for conservation tillage. However, due to the limited operating area of the straight blade set, it was not possible to effectively break soil blocks and stubbles (Figure 12b). The wing-shaped blade had both tangent and side blades, which allowed it to cut soil blocks and stubbles twice in one rotation cycle and break them into two small strip-shaped pieces (Figure 11c). Therefore, it increased the soil breakage rate. The straight blades on both sides of the wing-shaped blade set separated the inside and outside of the strip tillage area, so that the soil blocks and stubbles were constrained and broken in the strip tillage area (Figure 11c). In addition, the wing-shaped blade did not have a bending structure, so the amount of soil thrown outside the strip tillage area was lower. Therefore, it made the soil disturbance lower. In summary, wing-shaped blade sets were more suitable for strip no-tillage.

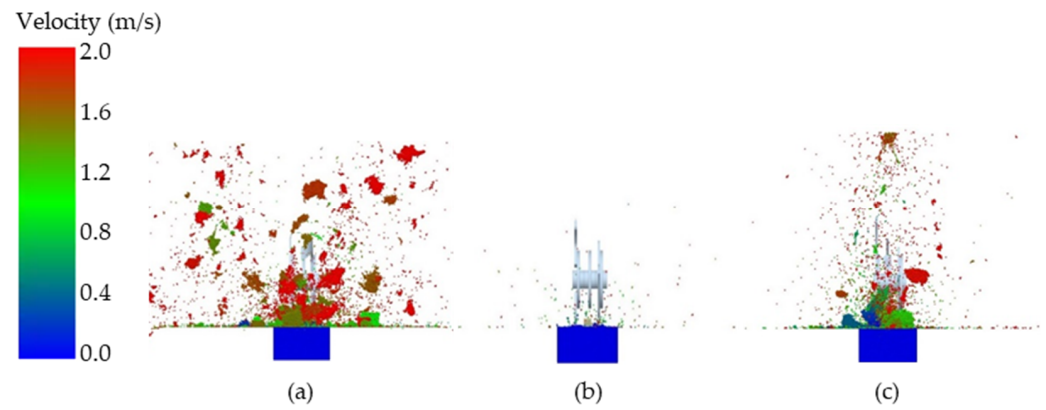


Figure 10. The soil movement of the (a) bent blade set, (b) straight blade set, and (c) wing-shaped blade set after the stubble-breaking operation.

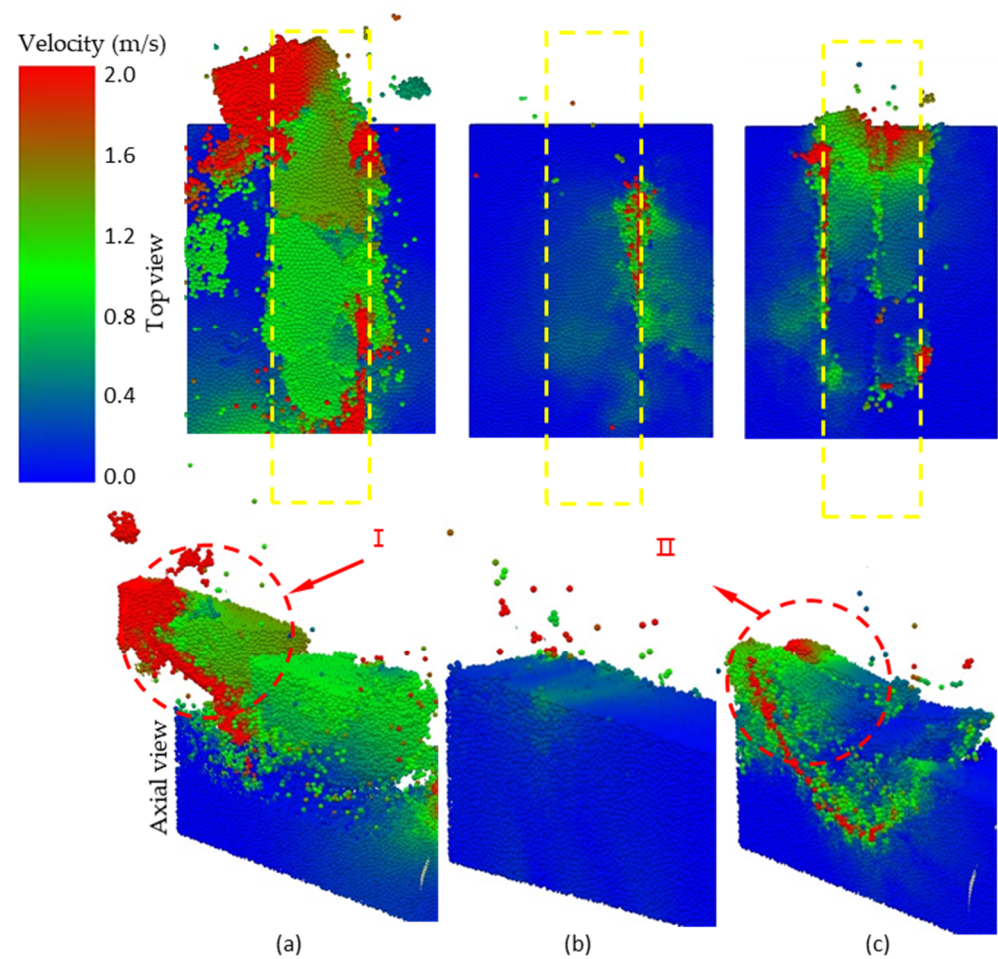


Figure 11. The soil blocks of the (a) bent blade set: I: large soil blocks; (b) straight blade set; and (c) wing-shaped blade set: II: strip-shaped soil blocks after the stubble-breaking operation.

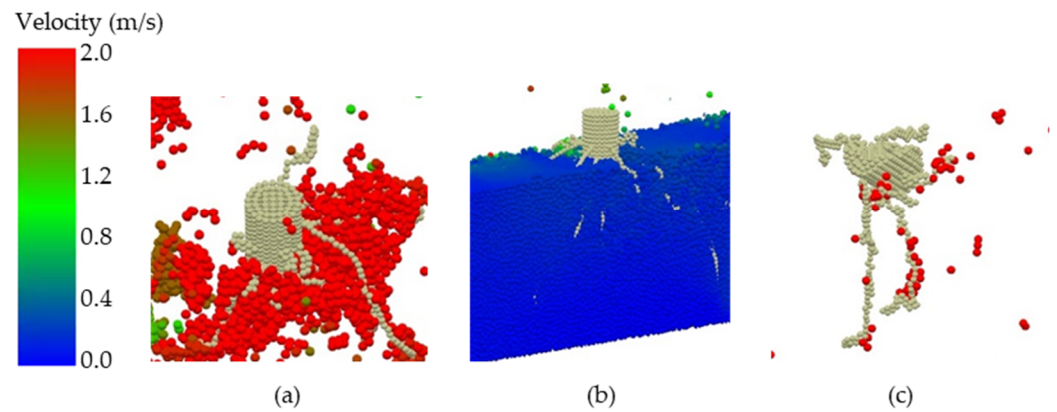


Figure 12. The stubble of the (a) bent blade set, (b) straight blade set, and (c) wing-shaped blade set after the stubble-breaking operation.

Liu et al. [30] found that as the number of roots in contact with the blade and the deflection of the roots increased, the blade resistance increased. As shown in the discrete element mechanics cloud diagram in Figure 13, compared to the straight blade, the bent blade had a longer blade edge. Therefore, the number of roots in contact with the bent blade was greater in one rotation cycle, resulting in a higher torque and more roots being cut. Compared to the bent blade, the straight blade had a greater slide cutting angle. Therefore, its stubble-breaking ability was stronger, which made roots fracture under a lower deformation, resulting in a minimal torque. The wing-shaped blade had the advantages of a straight blade and a bent blade. Its side blade and tangent blade contacted stubbles one after another and could cut the stubble twice. Therefore, although the wing-shaped blade had an additional set of blades, its torque was still at a low level, and it had good stubble-breaking performance.

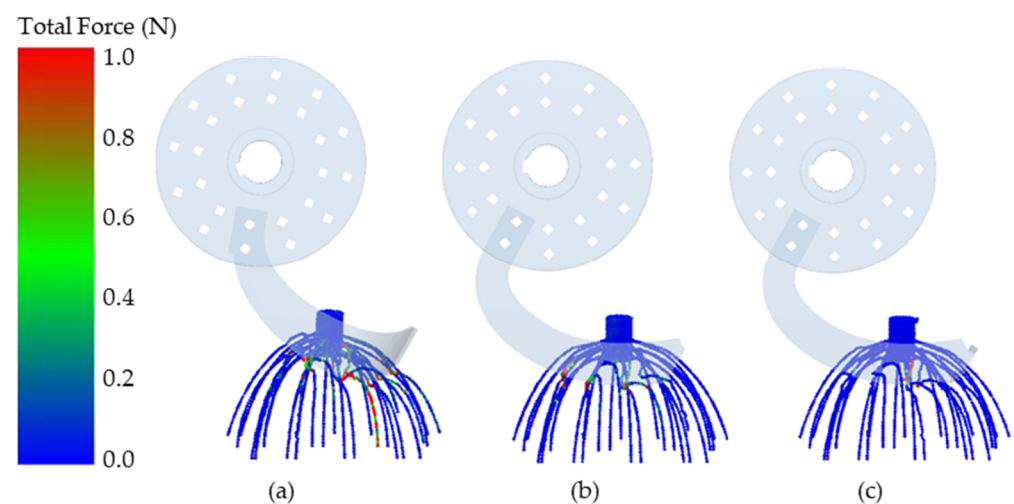


Figure 13. Interaction between maize roots and blade set: (a) bent blade set, (b) straight blade set, and (c) wing-shaped blade set.

5.1.2. Response Surface Test Result Analysis

To obtain the optimal performance of the wing-shaped blade, the Box–Behnken design method was used to optimize the design parameters, and the optimal parameter combination was determined. The results of the analysis of variance (ANOVA) are shown in Table 5. According to the experimental results, quadratic polynomial regression models for Y_1 , Y_2 , and Y_3 could be established, and the optimal working parameters could be determined.

Table 5. The results of the response surface test.

Num	X ₁	X ₂	X ₃	Y ₁	Y ₂	Y ₃
1	1	−1	0	49.14	77.46%	78.61%
2	1	0	−1	43.83	82.37%	67.65%
3	0	1	1	38.83	76.87%	70.06%
4	0	1	−1	45.75	82.87%	57.90%
5	0	0	0	40.68	77.84%	69.01%
6	0	0	0	39.68	78.51%	71.21%
7	0	0	0	38.68	79.07%	73.21%
8	−1	0	1	39.80	73.43%	64.93%
9	1	1	0	44.01	81.29%	67.09%
10	−1	−1	0	50.13	77.04%	71.68%
11	0	−1	−1	48.81	81.31%	76.86%
12	−1	1	0	47.87	78.69%	54.58%
13	0	−1	1	43.44	71.89%	78.20%
14	1	0	1	41.12	75.01%	77.69%
15	−1	0	−1	48.87	80.77%	60.62%

As shown in Table 6, if the *p*-value of Y₁ was less than 0.05, it indicated that the regression model was significant. If the *p*-value of the sum of squared residuals was greater than 0.05, it indicated that the regression model had a high degree of fit. The R² value was 0.99, indicating a high fit of the regression model to the sample. This regression model was used to predict and analyze the average torque of wing-shaped blade sets. According to the statistical analysis of Y₁, at the *p* < 0.01 level, X₁, X₂, X₃, X₁X₃, X₁², and X₂² were extremely significant (*p* < 0.05), while the others were not significant. The order of significance of the influence of various factors on the average torque was X₃ > X₂ > X₁. The insignificant regression terms (*p* > 0.05) in the model were removed, and the optimized model is expressed in Equation (13).

$$Y_1 = 39.72 - 1.07X_1 - 1.88X_2 + 3.01X_3 - 1.59X_1X_3 + 3.65X_1^2 + 4.45X_2^2 \tag{13}$$

Table 6. ANOVA results for the average torque.

Source	Sum of Squares	df	Mean Square	F	<i>p</i>
Model	237.69	9	26.41	59.97	0.0001
X ₁	9.18	1	9.18	20.84	0.006
X ₂	28.33	1	28.33	64.35	0.0005
X ₃	72.44	1	72.44	164.52	<0.0001
X ₁ X ₂	2.06	1	2.06	4.67	0.0831
X ₁ X ₃	10.08	1	10.08	22.89	0.005
X ₂ X ₃	0.60	1	0.60	1.36	0.2965
X ₁ ²	49.31	1	49.31	111.99	0.0001
X ₂ ²	73.3	1	73.30	166.46	<0.0001
X ₃ ²	0.019	1	0.019	0.044	0.8428
Residual	2.2	5	0.44		
Lack of Fit	0.20	3	0.067	0.067	0.9723
Pure Error	2	2	1		
Cor Total	239.89	14			

As shown in Table 7, if the *p*-value of Y₂ was less than 0.05, it indicated that the regression model was significant. If the *p*-value of the sum of squared residuals was greater than 0.05, it indicated that the regression model has a high degree of fit; the R² value was 0.99, indicating a high fit of the regression model to the sample. This regression model could be used to predict and analyze the soil breakage rate of wing-shaped blades. According to the statistical analysis of Y₂, at the *p* < 0.01 level, X₁, X₂, X₃, and X₂X₃ were extremely significant (*p* < 0.05), while the others were not significant. The order of

significance of the influence of various factors on the soil breakage rate was $X_3 > X_2 > X_1$. The insignificant regression terms ($p > 0.05$) in the model were removed, and the optimized model is expressed in Equation (14).

$$Y_2 = 0.78 + 0.77X_1 + 1.5X_2 + 3.76X_3 - 0.85X_2X_3 \tag{14}$$

Table 7. ANOVA results for the soil breakage rate.

Source	Sum of Squares	df	Mean Square	F	p
Model	141.49	9	15.72	81.36	<0.0001
X_1	4.78	1	4.78	24.76	0.0042
X_2	18.08	1	18.08	93.59	0.0002
X_3	113.35	1	113.35	586.6	<0.0001
X_1X_2	1.19	1	1.19	6.14	0.056
X_1X_3	0.0001	1	0.0001	0.0004	0.9849
X_2X_3	2.91	1	2.91	15.06	0.0116
X_1^2	0.035	1	0.035	0.18	0.6891
X_2^2	0.22	1	0.22	1.13	0.3355
X_3^2	0.86	1	0.86	4.45	0.0887
Residual	0.97	5	0.19		
Lack of Fit	0.21	3	0.069	0.18	0.9005
Pure Error	0.76	2	0.38		
Cor Total	142.46	14			

As shown in Table 8, if the p -value of Y_3 was less than 0.05, it indicated that the regression model was significant. If the p -value of the sum of squared residuals was greater than 0.05, it indicated that the regression model had a high degree of fit; the R^2 value was 0.98, indicating a high fit of the regression model to the sample. This regression model could be used to predict and analyze the soil backfill rate of wing-shaped blades. According to the statistical analysis of Y_3 , at the $p < 0.01$ level, X_1 , X_2 , X_3 , X_2X_3 , and X_1^2 were extremely significant ($p < 0.05$). The order of significance of the influence of various factors on the soil backfill rate was $X_2 > X_1 > X_3$. The insignificant regression terms ($p > 0.05$) in the model were removed, and the optimized model is expressed in Equation (15).

$$Y_3 = 70.92 + 4.9X_1 - 6.96X_2 - 3.48X_3 - 2.7X_2X_3 - 3.07X_1^2 \tag{15}$$

Table 8. ANOVA results for the soil backfill rate.

Source	Sum of Squares	df	Mean Square	F	p
Model	757.84	9	84.2	45.66	0.0003
X_1	192.32	1	192.32	104.28	0.0002
X_2	387.87	1	387.87	210.31	<0.0001
X_3	96.95	1	96.95	52.57	0.0008
X_1X_2	7.77	1	7.77	4.21	0.0953
X_1X_3	8.21	1	8.21	4.45	0.0886
X_2X_3	29.24	1	29.24	15.86	0.0105
X	35.31	1	35.31	19.15	0.0072
X_2^2	0.01	1	0.013	0.0071	0.9359
X_3^2	0.39	1	0.39	0.21	0.6635
Residual	9.22	5	1.84		
Lack of Fit	0.39	3	0.13	0.030	0.9911
Pure Error	8.83	2	4.41		
Cor Total	767.06	14			

Figure 14 shows the response surface of interaction factors for the average torque, soil breakage rate, and soil backfill rate. Figure 14a shows that the average torque first decreased and then increased as the slide cutting angle and pitching angle increased. Figure 14b shows that the average torque decreased first and then increased as the slide cutting angle increased. The average torque increased with the increase in wing width. Figure 14c shows that as the pitching angle increased, the average torque first decreased and then increased. The average torque increased with the increase in wing width.

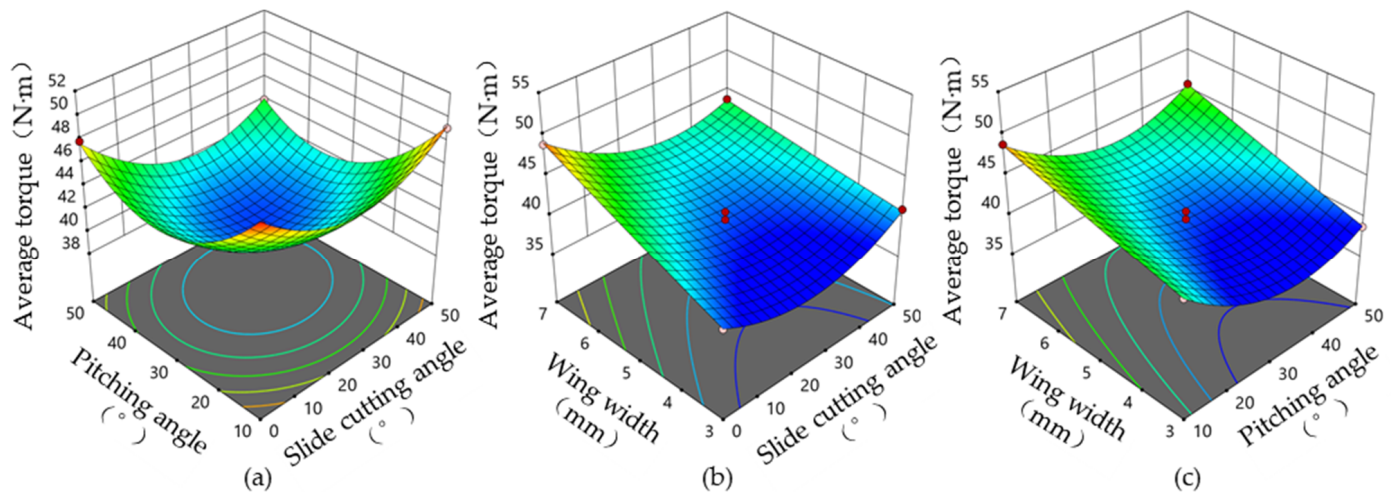


Figure 14. Response surface of different design parameters and average torque: (a) response surface of pitching angle, slide cutting angle and average torque; (b) response surface of wing width, slide cutting angle and average torque; (c) response surface of wing width, pitching angle and average torque.

The increase in the slide cutting angle resulted in a lower average torque [15]. However, as the slide cutting angle decreased, the length of the blade edge increased, and multiple blades entered the soil at the same time. Since the torque of the blade set was the sum of each blade's torque, the blade set with a large slide cutting angle had a higher torque. As the pitching angle increased, the area of the blade facing the soil increased, resulting in an increase in the average torque [33]. As the pitching angle decreased, the area of the blade facing the soil decreased, resulting in a decrease in the average torque. However, as the pitching angle continued to decrease, the wing contacted untilled soil, resulting in an increase in the average torque [32]. Similarly, as the wing width increased, the area of the blade facing the soil and the number of roots increased, resulting in a higher average torque.

Figure 15a shows that the soil breakage rate increased with the increase in the slide cutting angle and pitching angle. Figure 15b shows that the soil breakage rate increased with the increase in the slide cutting angle and wing width. Figure 15c shows that the soil breakage rate increased with the increase in the pitching angle and wing width.

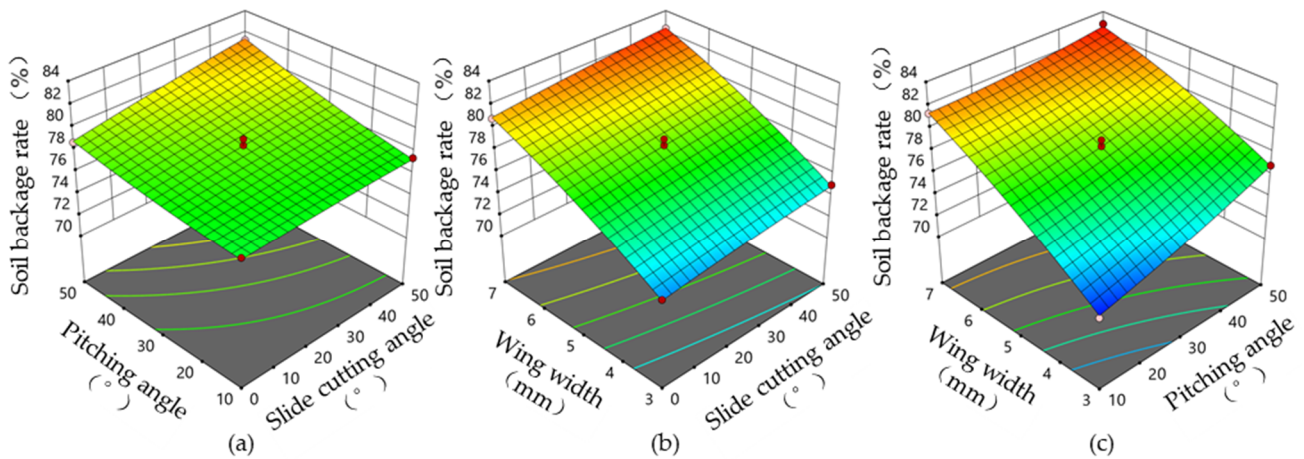


Figure 15. Response surface of different design parameters and soil breakage rate: (a) response surface of pitching angle, slide cutting angle and soil breakage rate; (b) response surface of wing width, slide cutting angle and soil breakage rate; (c) response surface of wing width, pitching angle and soil breakage rate.

The increase in the slide cutting angle caused the slide cutting phenomenon to occur, which made the stubbles and soil blocks more easily broken [15]. Therefore, the soil breakage rate increased with the increase in the slide cutting angle. As the pitching angle and wing width increased, the area of the blade facing the soil and stubbles would increase. More soil blocks and stubbles with kinetic energy would collide with the retaining plate, resulting in a higher soil breakage rate.

Figure 16a shows that the soil backfill rate decreased with the increase in the pitching angle and increased with the increase in the slide cutting angle. Figure 16b shows that the soil backfill rate increased with the increase in the slide cutting angle and decreased with the increase in the wing width. Figure 16c shows that the soil backfill rate decreased with the increase in the pitching angle and wing width.

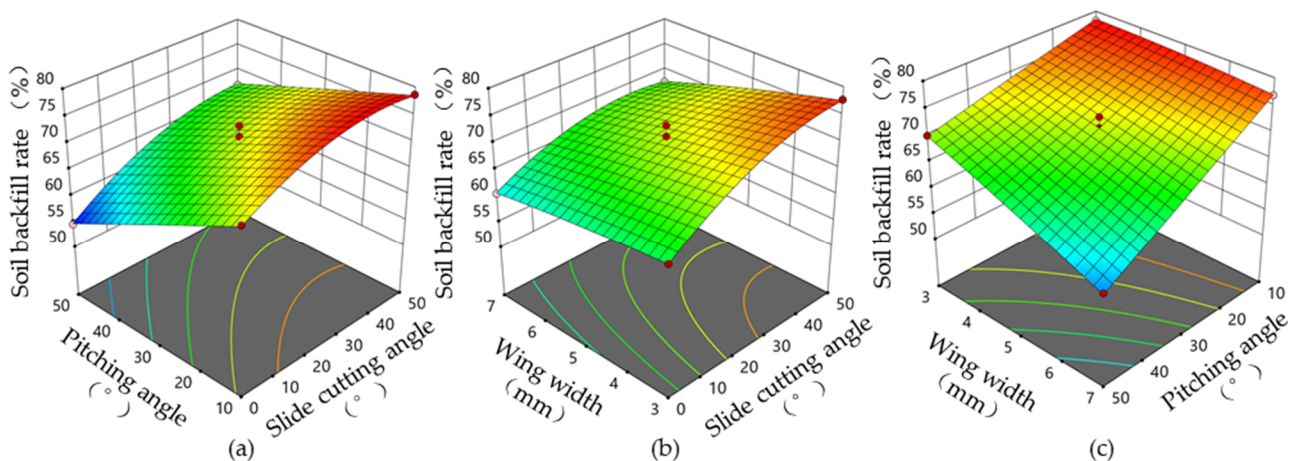


Figure 16. Response surface of different design parameters and soil backfill rate: (a) response surface of pitching angle, slide cutting angle and soil backfill rate; (b) response surface of wing width, slide cutting angle and soil backfill rate; (c) response surface of wing width, pitching angle and soil backfill rate.

The increase in the slide cutting angle resulted in less soil disturbance [15]. Therefore, larger slide cutting angles resulted in a higher soil backfill rate. However, as the slide cutting angle increased at a constant rate, multiple blades of the blade set would enter the soil at the same time, which would give the soil more kinetic energy [33]. The soil would

be thrown out of the strip tillage area, resulting in a lower soil backfill rate. As the pitching angle and wing width increased, the area of the blade facing the soil and stubbles would increase. More soil blocks and stubbles with kinetic energy would be thrown out of the strip tillage area, resulting in a decrease in the soil backfill rate.

It would be obvious that there were optimal values for the slide cutting angle, pitching angle, and wing width to make the wing-shaped stubble-breaking device have the optimal performance.

5.1.3. Optimization of Design Parameters

To obtain the optimal design parameters of the wing-shaped blade set, a multi-objective optimization was carried out based on the constructed regression model for the average torque, soil breakage rate, and soil backfill rate. The optimization objective function and constraint conditions were as follows:

$$\begin{cases} \min Y_1(X_1, X_2, X_3) \\ \max Y_2(X_1, X_2, X_3) \\ \max Y_3(X_1, X_2, X_3) \\ s, t. \begin{cases} 0 < X_1 < 50 \\ 10 < X_2 < 50 \\ 3 < X_3 < 7 \end{cases} \end{cases} \quad (16)$$

The optimization results of each design parameter were as follows: when the slide cutting angle, pitching angle, and wing width were 37° , 31° , and 50 mm, the average torque, soil breakage rate, and soil backfill rate were 40.13 N·m, 79.34%, and 71.81%.

5.2. Field Experiment Analysis

The results of the field experiment are shown in Figure 17. The average torque of the wing-shaped stubble-breaking device was 41.26 N·m, the soil breakage rate was 85.68%, and the soil backfill rate was 71.65%. Compared to the straight blade set, the wing-shaped blade set increased the average torque by 26.04% and the soil breakage rate by 51.96% and decreased the soil backfill rate by 5.03%; compared to the bent blade set, the wing-shaped blade set increased the average torque by 6.54%, the soil breakage rate by 9.48%, and the soil backfill rate by 28.08%. Overall, the wing-shaped blade set has the best stubble-breaking performance.

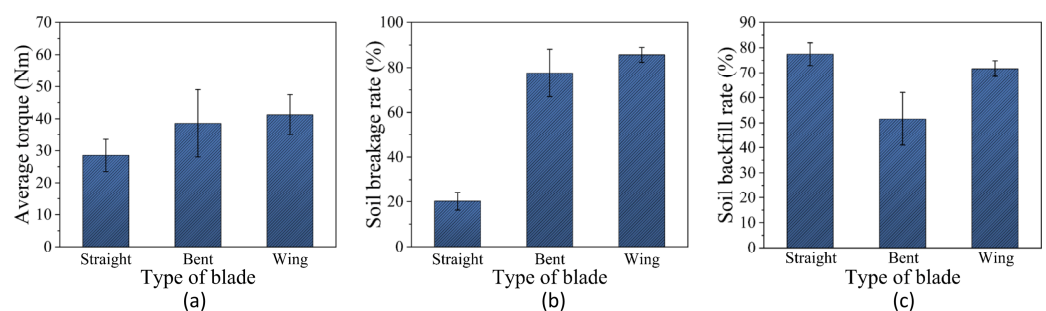


Figure 17. The influence of blade types on (a) the average torque, (b) soil breakage rate, and (c) soil backfill rate.

The straight blade set often left pancake-like stubbles and large soil blocks that were difficult to break (Figure 18a), which affected subsequent seeding. This was consistent with the results of discrete element analysis. Obviously, the straight blade set was not conducive to stubble-breaking operations.

The bent blade set had a good effect on breaking stubbles and soil blocks, but the bottom of the ditch and the soil blocks were often smeared (Figure 18b), which was not conducive to creating an excellent seedbed. Yang et al. [9,10] also found a similar phenomenon. In addition, due to the complex working environment in the field and the

unstable operation of tractors, the seeding bed often had stubbles and soil blocks of different sizes. Therefore, the stubble-breaking performance was not stable and there was a large deviation in the experimental data. Increasing the rotational speed of the stubble-breaking device and reducing the forward speed will make the stubble-breaking performance of the stubble-breaking device more stable.

The wing-shaped blade set was able to create a clean seedbed (Figure 18c) with small soil blocks and stubbles. The seedbed was suitable for seeding. Therefore, the wing-shaped blade set was the best choice for making excellent seedbeds.

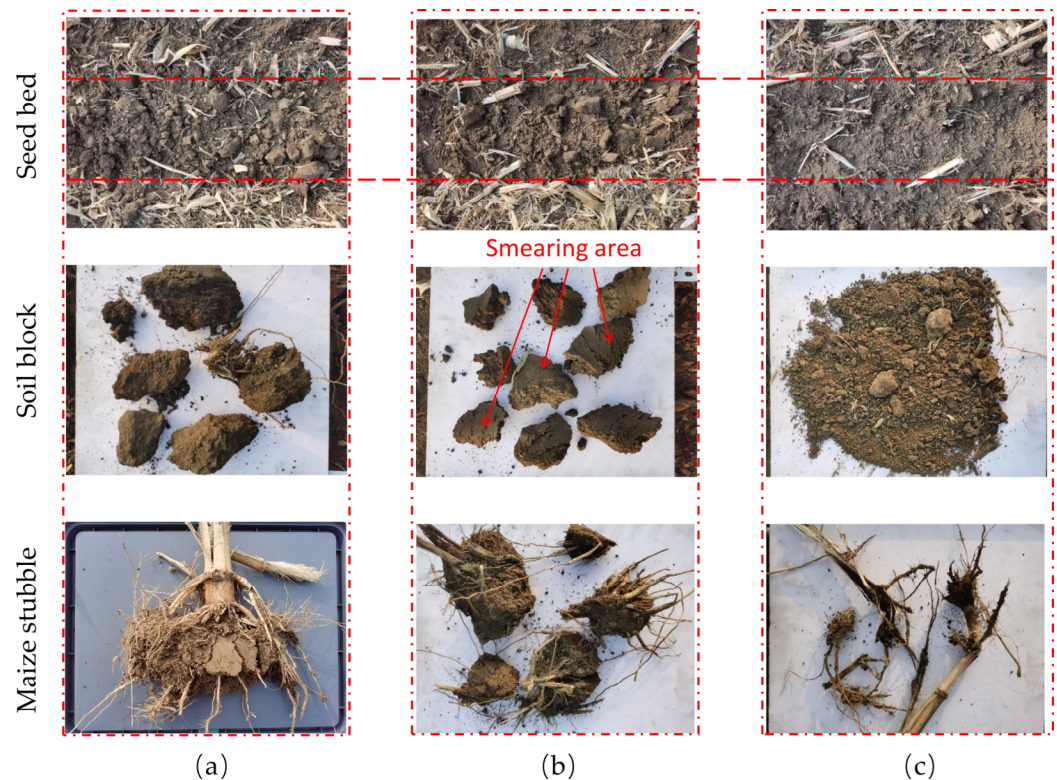


Figure 18. The shapes of the seeding bed, soil blocks, and maize stubbles of (a) the straight blade set, (b) bent blade set, and (c) wing-shaped blade set.

Although this study was able to optimize the design parameters of the tillage device within the allowable error range, the actual field environment is complex, and a large amount of straw and an uneven soil texture not only affect the performance of the tillage machine but also affect the prediction results. Therefore, in future research, developing accurate and complex farmland models deserves attention.

6. Conclusions

This study designed a wing-shaped stubble-breaking device for maize stubble. A DEM model of maize stubble was developed and used to optimize the design parameters of the stubble-breaking device. The interaction between stubble-breaking blades and the maize stubble was investigated using the DEM model. The DEM model was verified through soil bin tests and the performance of the wing-shaped stubble-breaking device was evaluated through field experiments. The results are as follows:

1. The verification experiment showed that the DEM model of maize stubble was accurate within the allowable error range. The optimization results of each design parameter were as follows: when the slide cutting angle, pitching angle, and wing width were 37° , 31° , and 50 mm, the average torque, soil breakage rate, and soil backfill rate were 40.13 N·m, 79.34%, and 71.81%.

2. As the slide cutting angle and pitching angle increased, the average torque first decreased and then increased; as the wing width increased, the average torque also increased; as the slide cutting angle, pitching angle, and wing width increased, the soil breakage rate also increased; as the slide cutting angle increased, the soil backfill first decreased and then increased; as the pitching angle and wing width increased, the soil backfill rate decreased.
3. The wing-shaped blade had both tangent and side blades, which allowed it to cut soil blocks and stubbles twice in one rotation cycle and break them into two small strip-shaped pieces. Therefore, it increased the soil breakage rate. The straight blades on both sides of the wing-shaped blade set separated the inside and outside of the strip tillage area so that the soil blocks and stubbles were constrained and broken in the strip tillage area. In addition, the wing-shaped blade did not have a bending structure, so the amount of soil thrown outside the strip tillage area was lower. Therefore, it made the soil disturbance lower. In summary, wing-shaped blade sets were more suitable for strip no-tillage.
4. The field experiment showed that the average torque of the wing-shaped stubble-breaking device was 41.26 N·m, the soil breakage rate was 85.68%, and the soil backfill rate was 71.65%. Compared with the straight blade set, the wing-shaped blade set increased the average torque by 13% and the soil breakage rate by 88.4%, and the soil backfill rate only decreased by 8.3%; compared to the bent blade set, the wing-shaped blade set increased the average torque by 1.24%, the soil breakage rate by 5.21%, and the soil backfill rate by 24.67%. Overall, the wing-shaped blade set has the best stubble-breaking performance.

This study provided an effective and feasible method for designing a stubble-breaking device and studying the interaction between blades, soil, and roots, which improved soil tillage theory and was beneficial in promoting conservation tillage technology. In future research, it will be necessary to conduct further studies on accurate and complex farmland environments.

Author Contributions: Conceptualization, X.L.; methodology, X.L.; software, X.L.; validation, X.L.; formal analysis, X.L.; investigation, X.L.; resources, Y.M.; data curation, X.L.; writing—original draft preparation, X.L.; writing—review and editing, X.L., H.Q., S.W., Z.X., P.G., D.F. and Y.M.; visualization, X.L.; supervision, Y.M.; project administration, Y.M.; funding acquisition, Y.M. All authors have read and agreed to the published version of the manuscript.

Funding: This work was supported by the National Natural Science Foundation of China [grant number 52275288], the National Key Research and Development Program of China [grant number 2023YFD2000903], and the Jilin Province Science and Technology Development Plan Item [grant number 20210202021NC].

Institutional Review Board Statement: Not applicable.

Data Availability Statement: The original contributions presented in the study are included in the article; further inquiries can be directed to the corresponding author.

Conflicts of Interest: The authors declare no conflicts of interest.

References

1. Wang, Q.; He, J. *Ridge Conservation Tillage*, 1st ed.; China Agricultural Science and Technology Press: Beijing, China, 2013.
2. Gao, W.; Zhang, H.; Chen, Y.; Chai, Q. *Conservation Farming System in China*, 1st ed.; China Agricultural University Press: Beijing, China, 2011.
3. He, J.; Li, H.; Chen, H.; Lu, C.; Wang, Q. Research Progress of Conservation Tillage Technology and Machine. *Trans. Chin. Soc. Agric. Mach.* **2018**, *49*, 1–19. [[CrossRef](#)]
4. Wang, Q.; Cao, X.; Wang, C.; Li, H.; He, J.; Lu, C. Research Progress of No/Minimum Tillage Corn Seeding Technology and Machine in Northeast Black Land of China. *Trans. Chin. Soc. Agric. Mach.* **2021**, *52*, 1–15. [[CrossRef](#)]
5. Zhang, X.; Jia, X.; Kang, M. *Manual of Agricultural Machinery*; Zhang, X., Ed.; China Agricultural Science & Technology Press: Beijing, China, 2007.
6. Zeng, D. *Mechanical Soil Dynamics*, 1st ed.; Beijing Science and Technology Press: Beijing, China, 1995.

7. Jia, H.; Guo, M.; Guo, C.; Zheng, J.; Zhang, C.; Zhao, J. Design of Dynamic Bionic Stubble Cutting Device and Optimization Test of Parameters. *Trans. Chin. Soc. Agric. Mach.* **2018**, *49*, 103–114. [[CrossRef](#)]
8. Jiang, J.; Gao, H. Corn Root Stalk and Residue Cutting Mechanism of No-Tillage Planter. *Trans. Chin. Soc. Agric. Mach.* **2004**, *20*, 129–131.
9. Yang, Y.; Ding, Q.; Zhao, Y.; Sun, C.; Wang, F. Optimization of the Rotary Tillage Tool for Wheat Strip-till Planter. *J. South China Agric. Univ.* **2021**, *42*, 110–115. [[CrossRef](#)]
10. Yang, Y.; Fielke, J.; Ding, Q.; He, R. Field Experimental Study on Optimal Design of the Rotary Strip-till Tools Applied in Rice-Wheat Rotation Cropping System. *Int. J. Agric. Biol. Eng.* **2018**, *11*, 88–94. [[CrossRef](#)]
11. Zhao, H.; Huang, Y.; Liu, Z.; Liu, W.; Zheng, Z. Applications of Discrete Element Method in the Research of Agricultural Machinery: A Review. *Agriculture* **2021**, *11*, 425. [[CrossRef](#)]
12. Zhao, W.; Chen, M.; Xie, J.; Cao, S.; Wu, A.; Wang, Z. Discrete Element Modeling and Physical Experiment Research on the Biomechanical Properties of Cotton Stalk. *Comput. Electron. Agric.* **2023**, *204*, 107502. [[CrossRef](#)]
13. Liu, W.; Zhang, G.; Wang, H.; Liu, H.; Kang, Q.; Zhao, Z.; Pei, L.; Li, Z. Microscopic Deformation and Fragmentation Energy Consumption Characteristics of Soils with Various Moisture Contents Using Discrete Element Method. *Soil Tillage Res.* **2024**, *241*, 106131. [[CrossRef](#)]
14. Su, Y.; Xu, Y.; Cui, T.; Gao, X.; Xia, G.; Li, Y.; Qiao, M. Determination and Interpretation of Bonded-Particle Model Parameters for Simulation of Maize Kernels. *Biosyst. Eng.* **2021**, *210*, 193–205. [[CrossRef](#)]
15. Zhao, H.; Li, H.; Ma, S.; He, J.; Wang, Q.; Lu, C.; Zheng, Z.; Zhang, C. The Effect of Various Edge-Curve Types of Plain-Straight Blades for Strip Tillage Seeding on Torque and Soil Disturbance Using DEM. *Soil Tillage Res.* **2020**, *202*, 104674. [[CrossRef](#)]
16. Song, W.; Jiang, X.; Li, L.; Ren, L.; Tong, J. Increasing the Width of Disturbance of Plough Pan with Bionic Inspired Subsoilers. *Soil Tillage Res.* **2022**, *220*, 105356. [[CrossRef](#)]
17. Wang, Y.; Zhang, D.; Yang, L.; Cui, T.; Jing, H.; Zhong, X. Modeling the Interaction of Soil and a Vibrating Subsoiler Using the Discrete Element Method. *Comput. Electron. Agric.* **2020**, *174*, 105518. [[CrossRef](#)]
18. Zeng, Z.; Chen, Y. Simulation of Straw Movement by Discrete Element Modelling of Straw-Sweep-Soil Interaction. *Biosyst. Eng.* **2019**, *180*, 25–35. [[CrossRef](#)]
19. Zeng, Z.; Ma, X.; Chen, Y.; Qi, L. Modelling Residue Incorporation of Selected Chisel Ploughing Tools Using the Discrete Element Method (DEM). *Soil Tillage Res.* **2020**, *197*, 104505. [[CrossRef](#)]
20. Zhang, S.; Zhao, H.; Wang, X.; Dong, J.; Zhao, P.; Yang, F.; Chen, X.; Liu, F.; Huang, Y. Discrete Element Modeling and Shear Properties of the Maize Stubble-Soil Complex. *Comput. Electron. Agric.* **2023**, *204*, 107519. [[CrossRef](#)]
21. Zhang, S.; Jia, X.; Dong, J.; Wang, X.; Zhao, H.; Chen, X.; Zhang, Z.; Huang, Y.; Shi, J. Optimization of Operating Angles of Disc Coulters for Maize Residue Management Using Discrete Element Method. *Comput. Electron. Agric.* **2024**, *218*, 108691. [[CrossRef](#)]
22. Zhang, S.; Huang, Y.; Zhao, H.; FU, Z.; Liu, Z.; Shi, J. Design and Experiment of Cutting and Throwing Combined Anti-Blocking Device for Wide-Seedbed Seeding of Wheat. *Trans. Chin. Soc. Agric. Mach.* **2024**, *55*, 40–52. [[CrossRef](#)]
23. Tamás, K.; Bernon, L. Role of Particle Shape and Plant Roots in the Discrete Element Model of Soil-Sweep Interaction. *Biosyst. Eng.* **2021**, *211*, 77–96. [[CrossRef](#)]
24. Qian, J.; Ma, S.; Xu, Y.; Li, W.; Wang, C.; Yang, S.; Wang, F. Experimental Study on the Sugarcane Stubble Base-Cutting Mechanism. *Biosyst. Eng.* **2024**, *245*, 122–134. [[CrossRef](#)]
25. Lee, K.S.; Park, S.H.; Park, W.Y.; Lee, C.S. Strip Tillage Characteristics of Rotary Tiller Blades for Use in a Dryland Direct Rice Seeder. *Soil Tillage Res.* **2003**, *71*, 25–32. [[CrossRef](#)]
26. Matin, M.A.; Desbiolles, J.M.A.; Fielke, J.M. Strip-Tillage Using Rotating Straight Blades: Effect of Cutting Edge Geometry on Furrow Parameters. *Soil Tillage Res.* **2016**, *155*, 271–279. [[CrossRef](#)]
27. Matin, M.A.; Fielke, J.M.; Desbiolles, J.M.A. Torque and Energy Characteristics for Strip-Tillage Cultivation When Cutting Furrows Using Three Designs of Rotary Blade. *Biosyst. Eng.* **2015**, *129*, 329–340. [[CrossRef](#)]
28. Matin, M.A.; Fielke, J.M.; Desbiolles, J.M.A. Furrow Parameters in Rotary Strip-Tillage: Effect of Blade Geometry and Rotary Speed. *Biosyst. Eng.* **2014**, *118*, 7–15. [[CrossRef](#)]
29. Matin, M.A.; Hossain, M.I.; Gathala, M.K.; Timsina, J.; Krupnik, T.J. Optimal Design and Setting of Rotary Strip-Tiller Blades to Intensify Dry Season Cropping in Asian Wet Clay Soil Conditions. *Soil Tillage Res.* **2021**, *207*, 104854. [[CrossRef](#)]
30. Liu, X.; Gao, P.; Qi, H.; Zhang, Q.; Guo, M.; Ma, Y. Interaction Mechanisms between Blades and Maize Root-Soil Composites as Affected by Key Factors: An Experimental Analysis. *Agriculture* **2024**, *14*, 1179. [[CrossRef](#)]
31. McKyes, E. *Agricultural Engineering Soil Mechanics*, 1st ed.; Distributors for the United States and Canada: New York, NY, USA, 1989.
32. Zhao, H.; He, J.; Li, H.; Liu, C.; Zheng, K.; Zhang, Z. Design and Experiment of Strip Rotary-Cut-Throw Anti-Blocking Implement. *Trans. Chin. Soc. Agric. Mach.* **2018**, *49*, 65–75. [[CrossRef](#)]
33. Gill, W.R.; Berg, G.E.V. *Soil Dynamics in Tillage and Traction*, 1st ed.; U.S. Government Printing Office: Washington, DC, USA, 1967.
34. Zhao, S.; Liu, H.; Yang, C.; Yang, L.; Gao, L.; Yang, Y. Design and Discrete Element Simulation of Interactive Layered Subsoiler with Maize Straw Returned to Field. *Trans. Chin. Soc. Agric. Eng.* **2021**, *52*, 75–87.

Disclaimer/Publisher’s Note: The statements, opinions and data contained in all publications are solely those of the individual author(s) and contributor(s) and not of MDPI and/or the editor(s). MDPI and/or the editor(s) disclaim responsibility for any injury to people or property resulting from any ideas, methods, instructions or products referred to in the content.